Eur. Phys. J. C (2025) 85:140
https://doi.org/10.1140/epjc/s10052-025-13871-1

THE EUROPEAN PHYSICAL JOURNAL C

Regular Article - Theoretical Physics

Prediction of mass and radii of anisotropic polytropic compact objects with Buchdahl-I metric

S. A. Mardan[1,a], **A. Zahra**[1,2,b], **Muhammad Bilal Riaz**[2,3,c], **Rubab Manzoor**[1,d], **Adnan Malik**[4,e]

[1] Department of Mathematics, University of the Management and Technology, C-II, Johar Town, Lahore 54590, Pakistan
[2] IT4Innovations, VSB-Technical University of Ostrava, Ostrava, Czech Republic
[3] Jadara University Research Center, Jadara University, Jordan
[4] University of Management and Technology, Sialkot campus, Pakistan

Received: 27 June 2024 / Accepted: 24 January 2025

Abstract In this article, we discuss several compact objects (GW 190814, PSR J0952-0607, PSR J0030+0451, PSR J0740+6620, GW 170817, PSR J1614-2230, PSR J2215+5135, and 4U 1608-52) to predict their masses and radii. A generalized polytropic stellar model within the framework of general relativity is derived by employing the Buchdahl-I metric. All the physical quantities such as energy density, radial, and tangential pressure are well behaved, continuous and no singularity is observed. The obtained results are compatible with observational data for compact objects under consideration. The physical stability of this model is determined by using generalized hydrostatic equilibrium condition, energy conditions, causality conditions and Herrera's cracking technique. We observe that our model fulfills all of the requirements for being a physically realistic model.

1 Introduction

Polytropes play a crucial role in astrophysics, particularly in modeling stellar structures. Many researchers used polytropic models to study internal stellar structures, astronomical phenomena, and compact objects (CO), highlighting the versatility and significance of polytropes in astrophysical research. The term polytrop refers to the solution of Lane–Emden equation, where density and pressure leads to polytropic EoS (EoS). Polytropes contribute significantly to the understanding and demonstration of the structure of CO and relativistic stars. Chandrasekhar [1] investigated the theory of polytropes within the Newtonian framework by applying the principles of thermodynamics. The solutions to the general relativity (GR) hydrostatic equations for a compressible fluid with spherical symmetry are discussed by Tooper [2]. He also obtain equilibrium equations that are related to the Lane–Emden equation in the Newtonian theory of polytropes. Komatsu et al. [3] investigated the numerical techniques for rapidly rotating general relativistic stars with uniformly rotating polytropes. Lane [4] proposed the polytropic EoS, can be used to defines pressure as a function of density, which simulate star structures in relativistic objects. Herrera et al. [5] used the polytropic EoS to analyze conformally flat and spherically symmetric fluid distributions. Kovetz [6] discussed the theory of slowly rotating polytropes and comprehended with the use of numerical results. Abramowicz [7] developed and explain the generic form of the Lane–Emden equation for the nth degree, which applies to spherical, cylindrical, and planar polytropes. Herrera and Barreto [8,9] presented a framework for anisotropic pressure modeling of polytropic Newtonian stars, derives the Lane–Emden equation, and uses a heuristic model to show the impacts of star structure.

Chavanis [10] explored cosmological models based on a generalized polytropic EoS and concluded that the universe can exist indefinitely into the future without encountering a singularity. Freitas and Gonçalves [11] studied the primordial Universe in a cosmological model where inflation is driven by a fluid with a polytropic EoS. The effect of generalized polytropic EoS on anisotropic polytropes with spherical and cylindrical symmetries was examined by Azam et al. [12]. Santana [13] developed a technique for solving the Lane–Emden equations in the context of relativistic

[a] e-mail: syedalimardanazmi@yahoo.com
[b] e-mail: F2019265004@umt.edu.pk;anam.zahra@vsb.cz (corresponding author)
[c] e-mails: muhammad.bilal.riaz@vsb.cz; bilalsehole@gmail.com
[d] e-mail: rubab.manzoor@umt.edu.pk
[e] e-mail: adnanmalik_chheena@yahoo.com

Published online: 04 February 2025

anisotropic polytropes with gravitational decoupling. Starting with a known Einstein field equations, the method simplifies computations and expands on known isotropic and anisotropic solutions. It significantly simplifies Tolman mass, especially with minimal geometric deformation, because one metric component remains constant. The method is demonstrated with Tolman IV, Durgapal IV, and Wymann IIa solutions. Urango [14] studied the generalized polytropes with relativistic anisotropic matter distribution. They determined the configurations' physical stability by integrating the relevant polytropic equation for different models. Godani, and Samanta [15] examined the neutron star model using GR and the polytropic EoS. The homotopy perturbation method is used to solve the Tolman–Oppenheimer–Volkoff (TOV) equation, which describes the mass distribution within a star's configuration. The model's stability, causality, and physical viability are examined, using observational results on known stars 4U 1608-52, SAX J1748.9-2021, RX J185635-3754, and 4U 1728-34.

The anionotropy factor is an important topic to explore while studying star formation. The study of anisotropic fluid is used to simulate the pressure components of CO. In GR, anisotropic fluids were extensively studied in spherical symmetry. Bower and Liang [17] used the generalized hydrostatic equilibrium condition (TOV equation) for relativistic objects to evaluate characteristics of anisotropic fluid distribution. Cosenza et al. [18] developed the heuristic procedure to obtain interior solutions to Einstein's equations by assuming anisotropic matter. The existence of local anisotropy in both Newtonian and general relativistic gravitationally bound system were examined by Herrera and Santos [19]. Herrera et al. [20] studied the behavior of self-gravitating spherically symmetric dissipative fluids with anisotropic stresses using the entire system of equations for general relativistic evolution. Herrera and Barreto [21] developed a framework for modeling Newtonian polytropes to demonstrate stellar structure. Reddy and his coworkers [22] investigated the development of a spherically symmetric stellar body under anisotropic stresses and heat dissipation during gravitational collapse. They found that the temperature and core instability of the collapsing bodies increased by pressure anisotropy. Bustos [23] explored the study of spherically symmetric COs with anisotropic matter using GR. The EoS of the generalized polytrope is used to prevent tangential velocity divergence at the object's surface. The polytropic equation is derived and integrated using an anisotropy function, and physical acceptability conditions are analyzed. A novel class of interior solutions for anisotropic COs with spherically symmetric matter distribution was introduced by Baskey et al. [24]. The exact solution for the field equation is obtained using a specific form of anisotropy. The Schwarzschild exterior metric over a compact star's bounding surface is used to determine the model parameters; pulsar 4U1608-52 is utilized for graphical representation. In both Newtonian and relativistic gravity, Cadogan and Poisson [25] introduced a theory of self-gravitating anisotropic fluids. They developed the Newtonian theory, inspired by the liquid crystal, and apply it to Newtonian stellar models. When they apply the theory to GR, they find that, for certain EoS and central density, anisotropic star models are less compact than isotropic. Sajadi et al. [26] studied the model consists of gravitating 3D spheres with an anisotropic fluid, corresponding to vacuum energy and a polytropic EoS. Using the TOV equation, three novel classes of asymptotically AdS black hole solutions with regular core are found. The regular behavior of these solutions is explained by repulsive gravity near the center. Stuchlík et al. [27] examined spherically symmetric equilibrium configurations of a perfect fluid with a polytropic EoS in spacetimes with a repulsive cosmological constant. These configurations, determined numerically, are bounded by a static radius and illustrated through embedding diagrams of spatial and optical geometries.

The stability analysis of CO plays a major role in mathematical modeling. Bondi [28] developed the hydrostatic equilibrium (TOV) equations to examine the stability of CO. Scientists have used both Schwarzschild and isotropic coordinates to develop mathematical models. Pandey et al. [29] used different polytropic index ranges to discuss the stability of stellar objects. The core-envelope model for spherically symmetric anisotropic CO was developed by Mardan et al. [30]. For the core, the polytropic EoS was taken into account, whereas the polytropic envelope was linear. Radial sound speed and the hydrostatic equilibrium conditions are used to determine the stability of the model.

The analysis of CO can provide theoretical insights into dense matter systems. Advances in theoretical modeling have made it easier to translate theoretical perspectives into analytical solutions. The choice of metric potential plays an important role in finding the analytical solutions for Einstein field equation (EFE). For evaluating the exact solutions of EFE, Delgaty and Lake [31] established metric ansatzes for the spherically symmetric distribution of ideal fluids in static regime. These solutions are useful for estimating CO's possible physical properties. For analyzing the characteristics of CO, the Buchdahl-I metric [32] is extremely helpful. Tamta and Fuloria [33] employ Buchdahl metric potential to investigate anisotropic stellar objects. They observed that the models retained the stability requirements across a range of parametric values. Maurya et al. [34] investigated anisotropic CO using the Buchdahl metric ansatz. They approximated EoS as a linear function of density.

The regime of stellar astrophysics is greatly influenced by the theory of gravity. More precisely, gravity theory predicts the existence of COs such as black holes, neutron stars, and white dwarfs and has a major influence on both the cosmic and galactic scales. In fact, the study and analysis of CO

plays an essential role in astrophysics because they serve as an excellent laboratory for studying dense matter under difficult circumstances, such as strong gravity. Romani et al. [35] investigated the mass of the Milky Way's fastest known spinning neutron star, pulsar PSR J0952-0607. This pulsar, whose spin period is $P = 1.41$ ms, was initially reported in [36]. It is a "black widow" pulsar, radiating and evaporating its low-mass companion due to the pulsar's brightness. PSR J0952-0607's mass measurement shows a maximum mass of 2.52 $M_\odot$ [35]. Miller et al. [37] studied the millisecond pulsar PSR J0030+0451, which spins at a frequency of 205.53 Hz, has been analyzed using Bayesian inference methods. This study estimate its mass as $1.44^{+0.15}_{-0.14}$ $M_\odot$ and its radius is $R = 13.02^{+1.24}_{-1.06}$ km. These measurements are essential for refining astrophysical constraints on the EoS of dense matter above nuclear saturation density. The millisecond pulsar MSP J0740+6620 has a mass of $2.14^{+0.1}_{-0.09}$ $M_\odot$, according to the most recent accurate estimation of a CO's maximal mass using Shapiro delay and recent studies of pulsars [38]. Das et al. [39] studied the models of anisotropic CO in Heintzmann geometry by introducing a pressure anisotropy parameter and solving Einstein's equations. For isotropic stars, the mass range is $1.87-3.04$ $M_\odot$ with radii between 8-13 km, while for anisotropic stars, the mass range is $1.99-3.23$ $M_\odot$. The model meets stability criteria and aligns with observed masses and radii of certain pulsars and gravitational wave companions. In the Buchdahl-I metric, Bhattacharjee and Chattopadhyay [40] explored about the maximal mass of an anisotropic CO that admits the modified Chaplygin EoS. They found that the maximum achievable mass is 3.72 $M_\odot$. In comparison with previously developed models, we can study more massive COs having maximum mass obtained through this model 3.86 $M_\odot$. Modified gravity theories have been extensively applied to compact stars, such as neutron and strange stars, to explore their structure and properties under alternative gravitational frameworks. These modifications, such as $f(R)$, $f(T)$, $f(R,T)$, $f(Q)$, and $f(R,G)$ gravity theories, help address discrepancies observed in gravitational dynamics and can influence key aspects like mass, radius, and stability. Many researchers work on modified gravity theories to study about the stellar objects [41–45]. We can also extend this work into modified theories of gravity.

The aim of this work is to develop a stellar model that represent the physical characteristics of anisotropic COs. These characteristics include anisotropy, radial and transverse pressures, mass, radius, and energy density (ρ). The mass and radii of the pulsars can be predicted by the model.

This research article outlined as follows. In Sect. 2, we consider a static spherically symmetric spacetime to find the EFEs with the help of the Buchdahl metric for the g_{rr} component as well as the polytropic EoS. The metric potential ν, tangential pressure (p_t), radial pressure (p_r), anisotropy factor ($\Delta = p_t - p_r$), and energy density (ρ) were all found in this section. To find the constants in the ansatz, we matched the inner solutions to the exterior geometry in Sect. 3. We illustrate the development of mass function in Sect. 4. We presented the radii and mass values of several recent pulsars in Tables 1 and 2. The graphical depiction of the essential elements of a stellar configuration, causality conditions, energy conditions are covered in Sect. 5. In Sect. 6, we analyze the model's stability using reliable techniques such as the generalized hydrostatic equilibrium condition (TOV equation) and Herrera's cracking technique. The results show that the model satisfies all relevant stability characteristics. We provide our final remarks in Sect. 7 to conclude the article.

Table 1 The values of mass function according to the constant H and $K = 10^{-5}$ km^2

H	$M(M_\odot)$	$R(km)$
0.20	1.77	7.18
0.30	2.21	8.79
0.40	2.56	10.05
0.50	2.78	11.10
0.56	2.98	11.66
0.60	3.05	11.99
0.70	3.26	12.78
0.80	3.48	13.48
0.90	3.72	14.16
1.00	3.86	14.72

2 Solutions to EFEs with generalized polytropic EoS

The following line element characterizes the static spherically symmetric space-time as

$$ds^2 = -e^{2\nu(r)}dt^2 + e^{2\lambda(r)}dr^2 + r^2(d\theta^2 + sin^2\theta d\phi^2). \quad (1)$$

The EFEs that link geometry and matter can be written as follows

$$R_{\alpha\beta} - \frac{1}{2}g_{\alpha\beta}R = 8\pi T_{\alpha\beta}. \quad (2)$$

The anisotropic representation of $T_{\alpha\beta}$ static matter distribution is provided as

$$T_{\alpha\beta} = \begin{bmatrix} -\rho & 0 & 0 & 0 \\ 0 & p_r & 0 & 0 \\ 0 & 0 & p_t & 0 \\ 0 & 0 & 0 & p_t \end{bmatrix}. \quad (3)$$

Table 2 Estimated radii from our model of several recently discovered pulsars and relativistic objects for $K = 10^{-5}$

CO	Measured mass ($M_\odot$)	Measured radius (km)	H=0.50	H=0.60	H=0.70	H=1.0
GW 190814 [46]	2.5−2.67	10.53−11.39	12.5	12.9	13.1	13.17
PSR J0952-0607 [48]	2.35 ± 0.17	14.087 ± 1.0816	11.85	12.30	12.60	12.75
PSR J0030+0451 [37]	$1.44^{+0.15}_{-0.14}$	$13.02^{+1.24}_{-1.06}$	9.45	9.60	9.70	10.03
PSR J0740+6620 [47]	2.08 ± 0.07	13-15	11.40	11.64	11.70	11.77
GW 170817 [49]	1.4	9.67-13	9.53	10.20	10.82	11.95
PSR J1614-2230 [50]	1.97 ± 0.04	13 ± 2	11.18	11.25	11.35	11.43
PSR J2215+5135 [51]	$2.27^{+0.17}_{-0.15}$	–	11.70	12.13	12.30	12.52
4U 1608-52 [52]	1.74 ± 0.14	9.3 ± 1.0	10.18	10.25	10.70	11.01

The EFEs are obtained by applying Eqs. (1) and (3) to Eq. (2) as

$$\frac{2e^{-2\lambda}\lambda'}{r} - \frac{e^{-2\lambda}}{r^2} + \frac{1}{r^2} = 8\pi\rho, \tag{4}$$

$$\frac{2e^{-2\lambda}\nu'}{r} + \frac{e^{-2\lambda}}{r^2} - \frac{1}{r^2} = 8\pi p_r, \tag{5}$$

$$e^{-2\lambda}\left(\nu'' - \lambda'\nu' + \nu'^2 - \frac{\lambda'}{r} + \frac{\nu'}{r}\right) = 8\pi p_t. \tag{6}$$

The derivative with respect to r is represented by $(')$. In this regard, the Buchdahl-I metric [32] is considered in way that described in [31]

$$e^{2\lambda(r)} = \frac{2 + 2\chi r^2}{2 - \chi r^2}, \tag{7}$$

where km^{-2} is the dimension of the constant χ. The energy density ρ is expressed by using Eq. (7) in Eq. (4)

$$\rho = \frac{3\chi(3 + \chi r^2)^{\ 2}}{16\pi(1 + \chi r^2)}. \tag{8}$$

The form of the generalized polytropic EoS is as follows [16]

$$p_r = H\rho + K\rho^{(2)}, \tag{9}$$

where n is the polytropic index, dimension of K is km^2 and H is dimensionless. Equations (7), (8), and (9) in Eq. (5) can be used to determine the value of the metric potential ν for $n = 1$.

$$\begin{aligned}\nu = -\frac{\chi}{192\pi}\Bigg(&\frac{6K(11 + 8r^2\chi)}{(1 + r^2\chi)^2} \\ &+ \frac{(48\pi(3 + 5H) + 25K\chi)log(r^2\chi - 2)}{\chi} \\ &- \Big(\frac{25K\chi + 96H\pi}{\chi}\Big)log(1 + r^2\chi)\Bigg).\end{aligned} \tag{10}$$

Similarly, radial and tangential pressure can be obtained as

$$p_r = \frac{3H\chi(3 + r^2\chi)}{16\pi(1 + r^2\chi)^2} + \frac{9K\chi^2(3 + r^2\chi)^2}{256\pi^2(1 + r^2\chi)^4}, \tag{11}$$

$$\begin{aligned}p_t = &\frac{1}{576\pi\chi^2(r^2\chi - 2)(1 + r^2\chi)^3(3 + r^2\chi)^2} \\ &\times\Big[-65536K^2\pi^4r^2(1 + r^2\chi)^8 \\ &+1536K\pi^2\chi(1 + r^2\chi)^4(12 + 3(9H + 16)r^2\chi \\ &+(18H + 5)r^4\chi^2 + (3H - 1)r^6\chi^3) \\ &-27\chi^3(3 + r^2\chi)^2(3H^2r^2\chi(3 + r^2\chi)^2 \\ &+3r^2\chi(3 + 4r^2\chi + r^4\chi^2) + 2H(12 + 8r^2\chi \\ &+17r^4\chi^2 + 3r^6\chi^3))\Big].\end{aligned} \tag{12}$$

The expression for total gravitational mass of sphere is given as

$$m(r) = 4\pi\int_0^R \rho r^2 dr. \tag{13}$$

3 Exterior spacetime and junction conditions

We will match the exterior Schwarzschild spacetime to the interior spacetime at the boundary surface to determine the continuity of metric potentials at boundary surface.

The external Schwarzschild metric is expressed as

$$ds^2 = -f(r)\,dt^2 + \frac{1}{f(r)}\,dr^2 + r^2\left(d\theta^2 + \sin^2\theta\,d\phi^2\right), \tag{14}$$

where the function $f(r)$ is defined as

$$f(r) = 1 - \frac{2M}{R}.$$

The continuity of the two metric potentials at the surface ($r = R$) of the CO results as

$$e^{2\nu} = e^{-2\lambda} = 1 - 2u, \tag{15}$$

where $u = \frac{M}{R}$ is the compactness factor of the star. The radial pressure is defined as zero at the boundary surface, i.e.,

$$p_r(R) = 0. \tag{16}$$

The expressions of constants χ and K can be obtained by using Eqs. (15), (7), (8) and (9)

$$\chi = \frac{4u}{R^2(3-4u)}, \tag{17}$$

$$K = \frac{16H\pi(-1-R^2\chi)^2}{3\chi(3+R^2\chi)}. \tag{18}$$

At the centre ($r = 0$), the pressure and energy density must be finite and positive. The central density can be expressed as follows using Eq. (8).

$$\rho_0 = \frac{9\chi}{16\pi} = \frac{4u}{4\pi R^2(3-4u)}. \tag{19}$$

The central pressure expression, derived from Eq. (11), is

$$p_r(0) = \frac{9H\chi}{16\pi} + \frac{81K\chi^2}{256\pi^2}. \tag{20}$$

The central energy density will only be positive if $\chi > 0$, according to Eq. (19). To ensure a positive central pressure in this model, the parameters H and K must satisfy specific constraints given by the condition

$$\frac{H}{K} > \frac{9\chi}{16\pi}, \tag{21}$$

indicating that the ratio $\frac{H}{K}$ is influenced by the compactness u and the radius R of the stellar object. We have selected H and K values in accordance with Eq. (21).

4 Mass-radius relation for polytropic model

Figure 1a–d displays the masses of COs calculated through this model for a range of values for H and K. As illustrated in Fig. 2, we have also solved the TOV equation together with the polytropic EoS to derive the mass-radius relation for COs. When $K = 10^{-5}$ km^2, the maximum mass of the CO changes from 1.77 $M_\odot$ to 3.86 $M_\odot$ due to the variation of the polytropic parameter H, as shown in Tab. (1). It is clear that using polytropic EoS may expand the maximal mass range, allowing COs to have more mass to resist their gravitational collapse. Thus, based on the most recent observations, a broad range of CO masses can be described. According to earlier research [40], 3.72 $M_\odot$ is hardly theoretically feasible mass in GR. Table 2 shows that changing the values of H and K use to predict the radii of pulsars. Therefore, the presented model can be used to estimate the radii of a studied COs.

5 Physical implementation of the model

The properties of COs will be illustrated graphically in this section. For this, we considered GW 190814, PSR J0952-0607, PSR J0030+0451, GW 170817, PSR J1614-2230, PSR J2215+5135, 4U 1608-52, and PSR J0740+6620 COs. The measured radii and masses of COs are given in Table 2, with compactness factors accordingly.

5.1 Causality conditions for stability analysis

The two velocities taken into account in the causality stability analysis are the tangential (v_t^2) and radial (v_r^2) speeds of sound. Sound speeds are calculated as follows Sound velocities' causality conditions implies an absolute upper bound for both $v_r^2 \leq 1$ and $v_t^2 \leq 1$. However, the thermodynamic stability guarantees that both v_r^2 and $v_t^2 > 0$. Thus, the criteria $0 \leq v_r^2 < 1$ and $0 \leq v_t^2 < 1$ should hold simultaneously inside the stellar composition. Because of the difficulty of the sound velocity equations, we have graphically depicted variations of v_r^2 and v_t^2 in Fig. 7a, b, respectively. Figure 7a, b make it clear that this model complies with the causality conditions.

5.2 Energy conditions

In order to generate a realistically feasible energy momentum tensor, the energy conditions are applied to matter distributions in gravitational theory. These conditions provide a means of obtaining qualitative information about the nature of matter distribution without requiring precise details about the internal matter content. Thus, by disregarding the energy density or pressure, one can explore the physical characteristics of extreme phenomena like gravitational collapse or the presence of geometric singularities. Within the stellar boundary, a physically realistic fluid distribution must satisfy the dominant energy condition (DEC), strong energy condition (SEC), weak energy condition (WEC), and null energy condition (NEC) [53–55].

For the current stellar model, we evaluated the energy conditions [56,57] and found that they are completely satisfied. Energy conditions must be satisfied both within and on the surface of a compact star for a model to be considered physically realistic [56,57]. We verified that the energy conditions

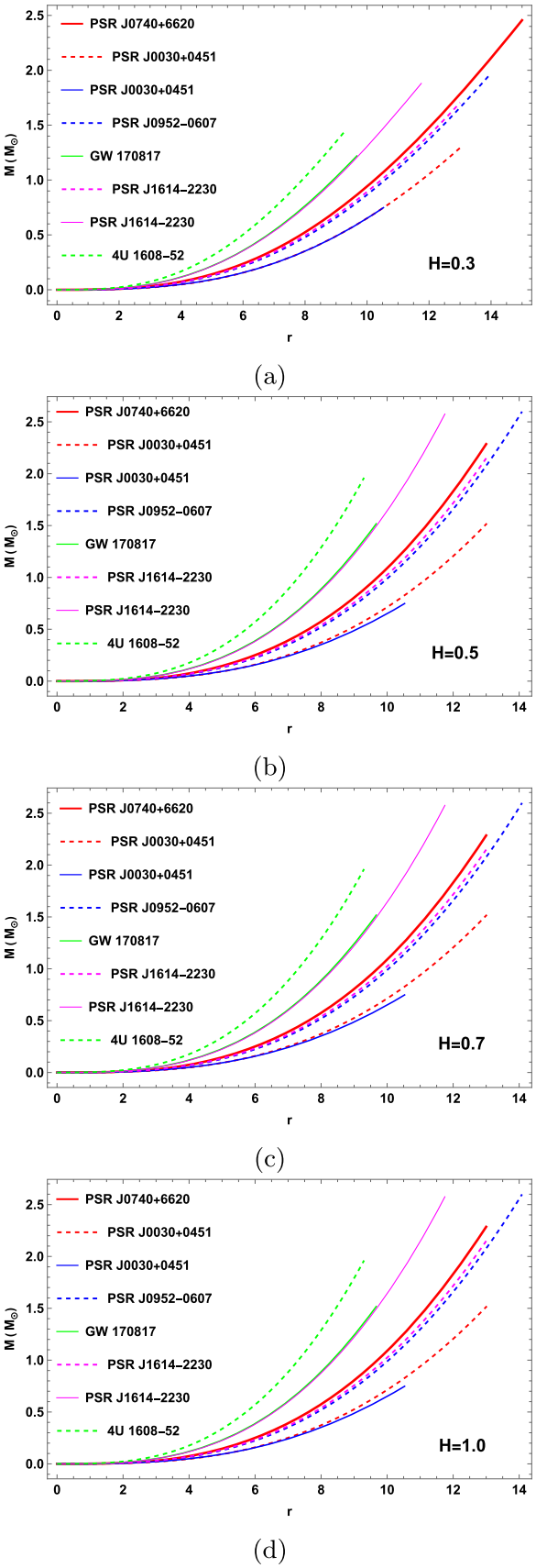

Fig. 1 Variation of masses against r

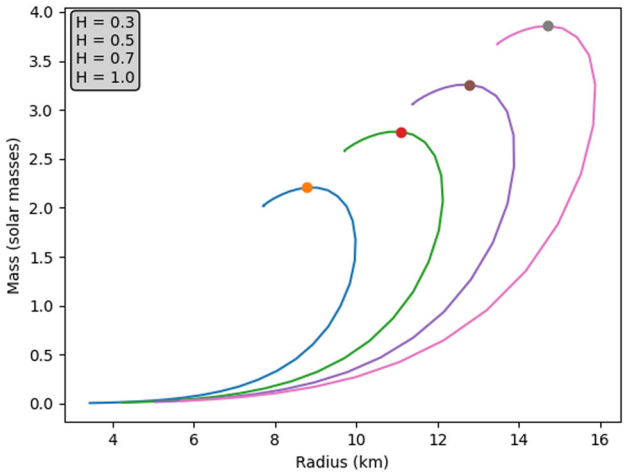

Fig. 2 The mass radius plot for $K = 10^{-5}$ km^2

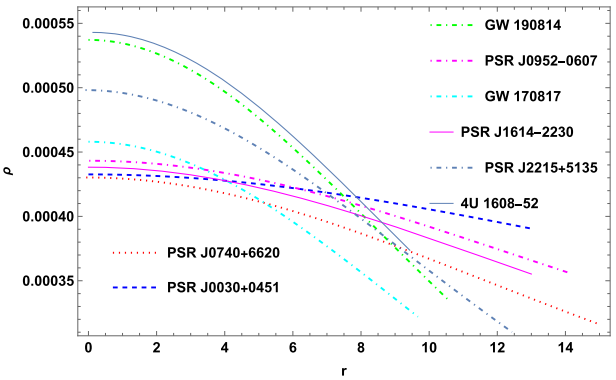

Fig. 3 The plot of energy density function for $H = 0.3$ and $K = 10^{-5}$ km^2

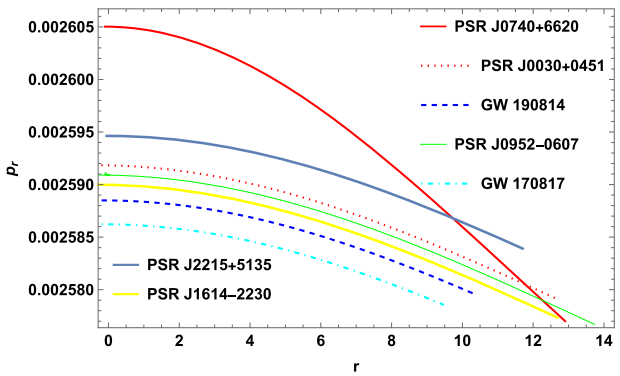

Fig. 4 The plot of radial pressure for $H = 0.3$ and $K = 10^{-5}$ km^2

for this model inside its parameter space are consistent with the below outlined conditions. The energy conditions are

- NEC: $\rho + p_r \geq 0$, $\rho + p_t \geq 0$.
- WEC: $\rho \geq 0$, $\rho + p_r \geq 0$, $\rho + p_t \geq 0$.
- SEC: $\rho + p_r \geq 0$, $\rho + p_t \geq 0$, $\rho + p_r + 2p_t \geq 0$.
- DEC: $\rho \geq 0$, $\rho - p_r \geq 0$, $\rho - p_t \geq 0$.

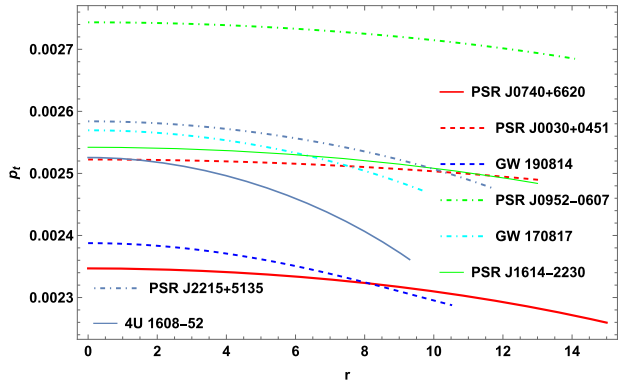

Fig. 5 The plot of tangential pressure for $H = 0.3$ and $K = 10^{-5}$ km^2

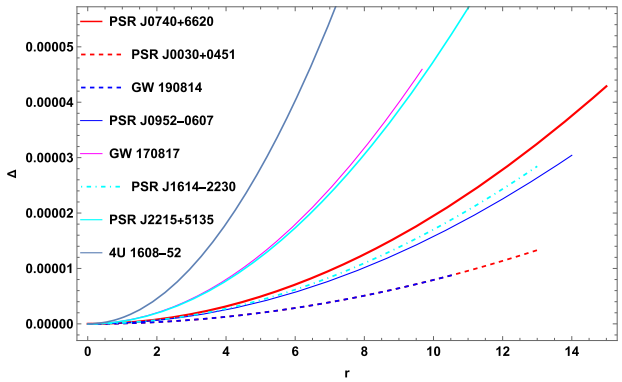

Fig. 6 The plot of anisotropy for $H = 0.3$ and $K = 10^{-5}$ km^2

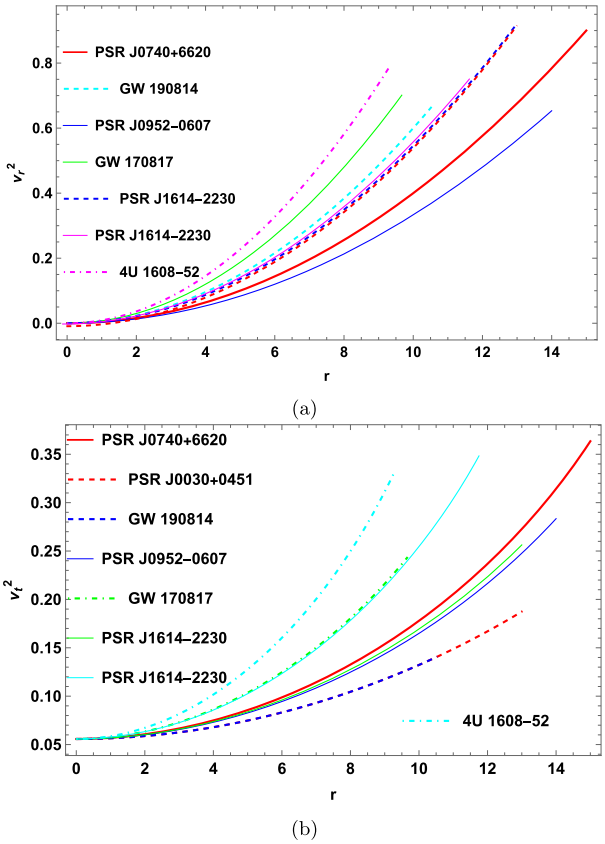

Fig. 7 Verification of causality conditions for $H = 0.3$ and $K = 10^{-5}$ km^2

The graphical representation of these conditions are given in Fig. 8a–h.

6 Stability analysis

Following techniques will be used to investigate the stability of model.

(i) Hydrostatic equilibrium condition (TOV equation)
(ii) Cracking technique

6.1 Hydrostatic equilibrium condition (TOV equation)

Analysis of hydrostatic equilibrium is essential for the investigation of model's stability under various forces. The stability for an anisotropic CO depends on the following forces the hydrostatic force F_h, the gravitational force F_g, and the anisotropic force F_a. Under the combined effect of these factors, the model supposed to be in equilibrium. The generalized hydrostatic equilibrium condition (TOV equation) [58,59] of the following form has been used to study the stability

$$-\frac{M_G(r)e^{\lambda-\nu}}{r^2}(\rho+p_r)-\frac{dp_r}{dr}+\frac{2\Delta}{r}=0, \tag{22}$$

where M_G represents the active gravitational mass, which can be determined from Tolman–Whittaker mass formula given in [60], described as

$$M_G(r)=r^2\nu' e^{\nu-\lambda}. \tag{23}$$

Eq. (23) is substituted into Eq. (22), yielding

$$-\nu'(\rho+p_r)-\frac{dp_r}{dr}+\frac{2\Delta}{r}=0. \tag{24}$$

These three forces can be represented as

$$F_g=-\nu'(\rho+p_r), \tag{25}$$

$$F_h=-\frac{dp_r}{dr}, \tag{26}$$

$$F_a=\frac{2\Delta}{r}. \tag{27}$$

The expressions of Eqs. (25)–(27) can be computed using Eqs. (8), (11), and (12). The graphical representation of the equilibrium conditions as presented in Fig. 9a–h.

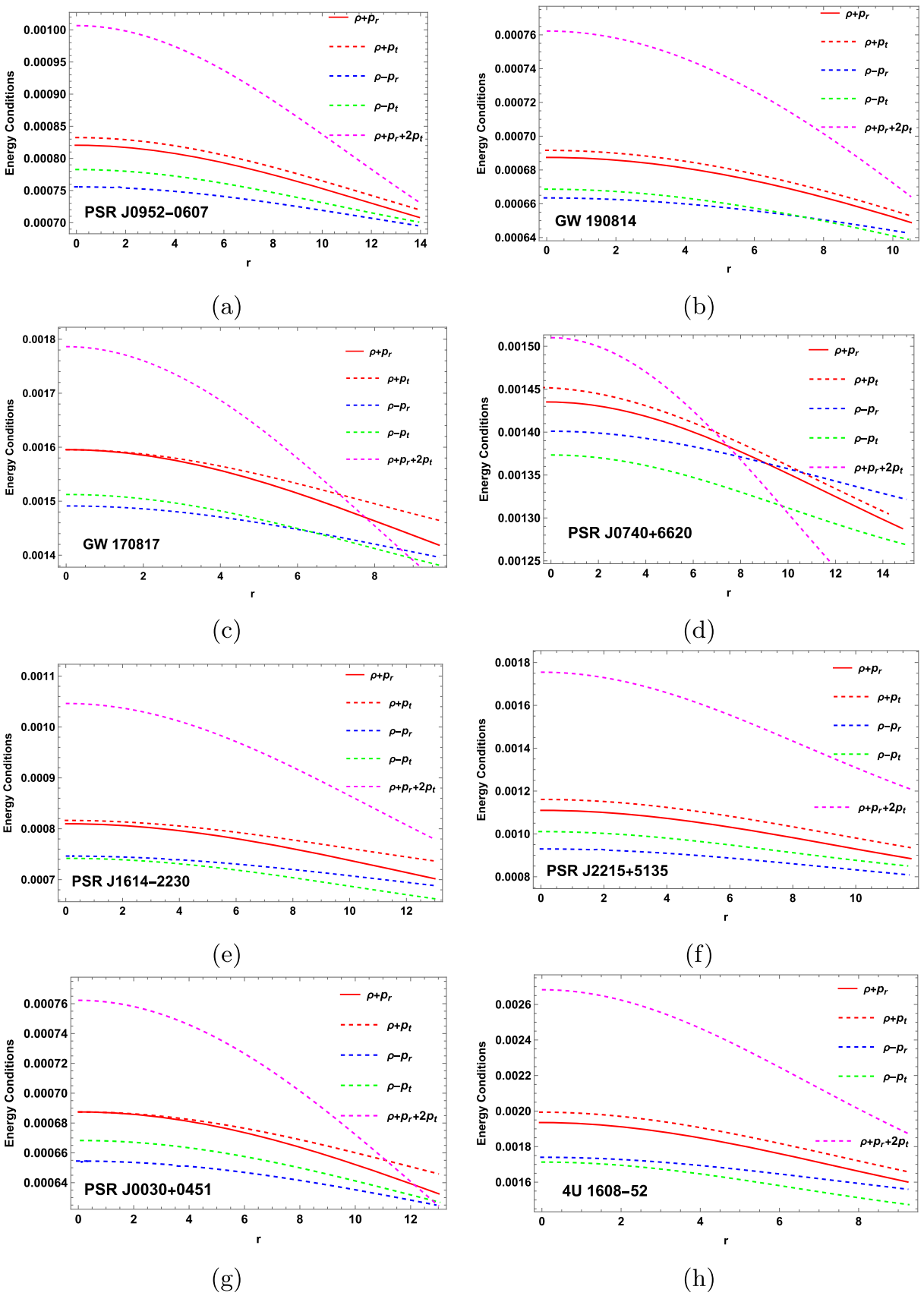

Fig. 8 Energy conditions against for $H = 0.3$ and $K = 10^{-5}$ km^2

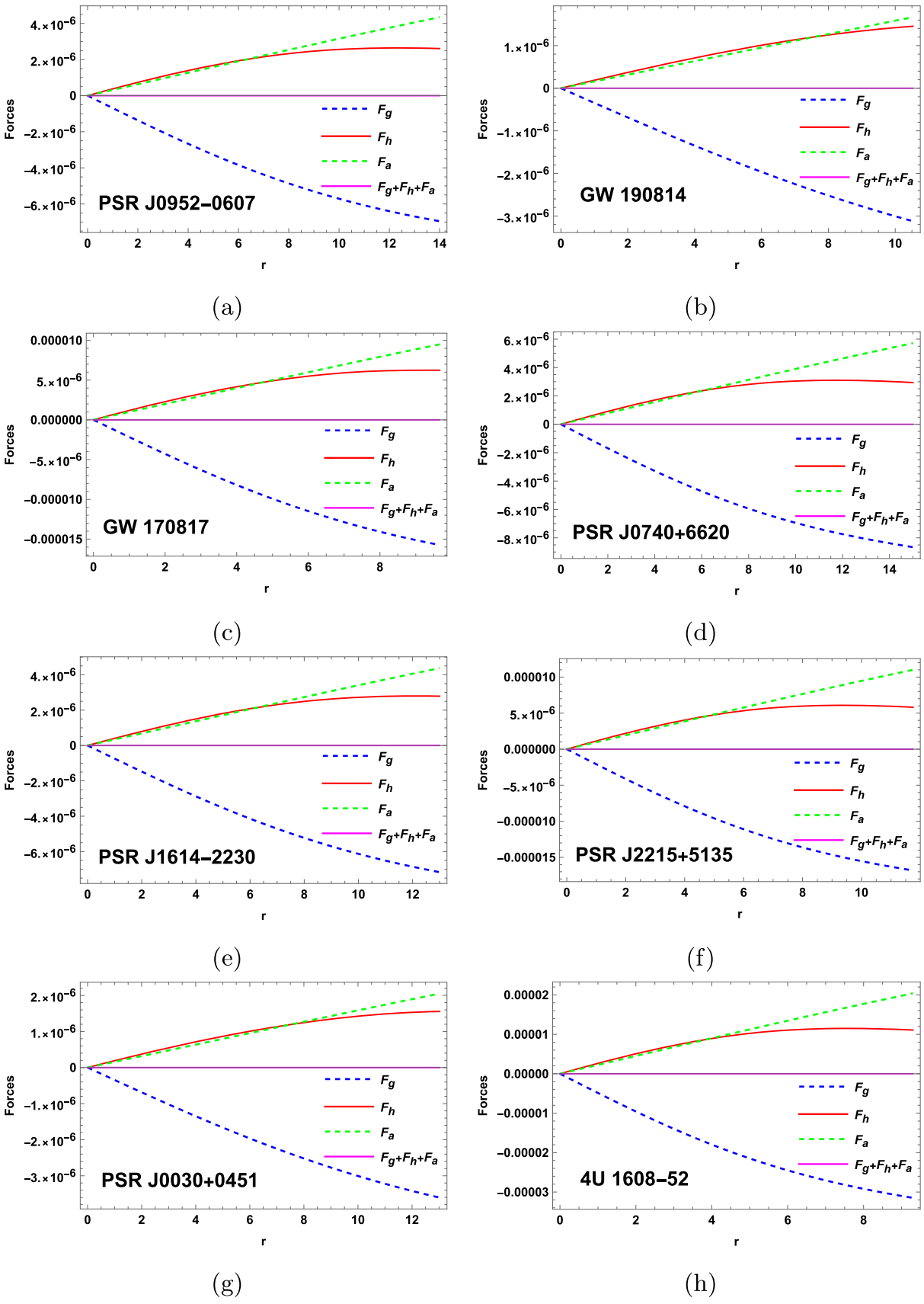

Fig. 9 Hydrostatic equilibrium of various objects for $H = 0.3$ and $K = 10^{-5}$ km^2

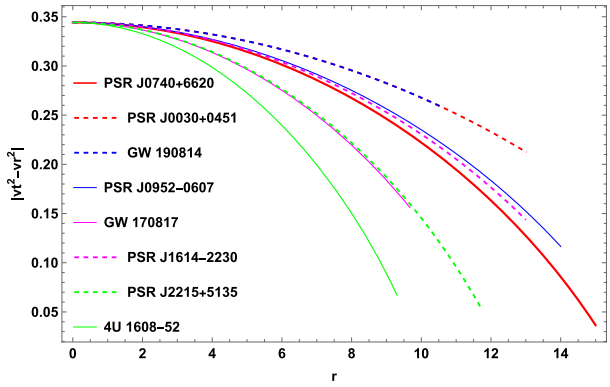

Fig. 10 $|v_t^2 - v_r^2|$ is plotted for $H = 0.3$ and $K = 10^{-5}$ km^2

6.2 Cracking technique

Herrera introduced cracking technique to discuss the stability of stellar models [61]. A criterion based on Herrera's technique was proposed by Abreu et al. [62] to determine the stability of an anisotropic star model by using radial and tangential sound speed velocities. Thus, if stellar models satisfy following condition

$$0 \leq |v_t^2 - v_r^2| \leq 1. \tag{28}$$

it can be considered as stable structure of COs. According to Fig. 10, the Eq. (28) meets the criteria for all points of GW 190814, PSR J0952-0607, PSR J0030+0451, PSR J0740+6620, GW 170817, PSR J1614-2230, PSR J2215+5135, and 4U 1608-52.

7 Conclusion

In this article a novel generalized model of anisotropic CO using polytropic EoS and the Buchdahl-I metric is present. The constant χ in Eq. (17) and K in Eq. (18) are derived from the metric functions at stellar boundaries. The positive limit of the central density is $\chi > 0$. Positive central pressure causes a correlation between constants H and K, as seen in Eq. (21).

Mass and radius: The plots of mass functions for COs under consideration are given in Fig. 1a–d. Table 1 shows how mass varies with the polytropic parameter H at $K = 10^{-5}$ km^2. The mass of COs ranges from $1.77-3.86$ and for radii from $7.18-14.72$ km as H changes from 0.2 to 1.00. To get a mass plot in this model, the value of H is constrained between 0.2 and 1.00. As H increases, so do both mass and radius. We may use current measurements to establish the mass range of lighter objects and pulsars using polytropic EoS. In addition, we projected the pulsars PSR J0952-0607, GW 190814, PSR J0030+0451, PSR J0740+6620, PSR J1614-2230, 4U 1608-52, and PSR J2215+5135, which are included in Table 2, as well as the companion star of the GW170817 event. Table 2 shows that different values of constants that help us to predict the radii of COs for corresponding mass ranges. Considering the significance of EoS in describing the characteristics of COs, it's possible that high mass pulsars may have polytopic EoS within their interiors.

Density, pressures and anisotropy: The solutions to the EFEs give us the expressions for density, radial pressure, tangential pressure, and anisotropy, as shown in Eqs. (8), (11), (12). It is evident from the Figs. 3, 4, and 5 energy density, radial and tangential pressure, with a maximum value at the center for $H = 0.3$ demonstrate feasible behavior. In Fig. 6, the anisotropy is minimal at the core and reaches its peak at the surface, highlighting the significant repulsive force caused by surface anisotropy in stellar objects. There is no observable singularity.

Causality conditions: Figure 7a, b for the radial and tangential components of sound speed satisfy the causality condition, respectively. At $H = 0.3$, these Fig. 7a, b confirm the viability of the stellar model.

Energy conditions: The anisotropic fluid distribution fulfills all energy conditions, including NEC, WEC, SEC, and DEC. We investigated these conditions for various pulsars, including PSR J0952-0607, GW 190814, PSR J0030+0451, PSR J0740+6620, PSR J1614-2230, 4U 1608-52, and PSR J2215+5135. Figure 8a–h shows that all energy conditions maximum in the core and gradually decrease towards the surface of the stellar objects.

Hydrostatic equilibrium condition: Equation (22) describes the hydrostatic equilibrium condition (TOV equation) for static, anisotropic fluids in a spherically symmetric sphere. Figure 9a–h show that the model is in equilibrium under gravitational, hydrostatic, and anisotropic forces.

Cracking technique: Figure 10 shows that it is well behaved and continuous, and no singularity is observed in our stellar models. The value reaches its maximum at the center and decreases gradually toward the surface as the radius increases.

The current model, based on generalized polytropic EoS, can accurately explain the mass and internal features of COs. It also provides a stable representation of anisotropic COs. Therefore, we can conclude the discussion by stating that our stellar models with anisotropic fluid distribution and modified Buchdhal-I metric potential provide a novel path for researchers to investigate ultra-dense COs. Rafelski et al. [63] investigated the characteristics and gravitational interactions of ultra-dense objects with masses comparable to meteors or greater, possessing nuclear-level densities. Their work examined the possibility of such objects being enclosed within comets, their stability upon impacting celestial bodies like Earth and the Sun, and the hypothesis of a core composed of ultra-dense matter. Similarly, Dietl et al. [64]

focused on gravitationally bound dark ultra-dense objects, analyzing their surface gravity, tidal forces, and the observable effects of their collisions with visible matter. Tamta [65] introduced a novel mass function aimed at addressing the field equations and constructing spherically symmetric models of ultra-dense stellar objects. Despite this advancement, the model lacks stability under the combined effects of hydrostatic, anisotropic, and gravitational forces, although it satisfies the causality condition within the fluid spheres. Carballo-Rubio [66] employed a numerical approach to study the characteristics of ultra-COs composed of an ideal isotropic fluid, governed by a straightforward yet physically realistic equation of state. Similarly, Cunha et al. [67] conducted fully nonlinear numerical simulations of ultra-compact bosonic stars that are stable against known instabilities. They introduced a new adiabatic effective potential method to investigate light-ring-induced instabilities, identifying two potential outcomes: either the object transitions to a non-ultra-compact configuration or it collapses into a black hole.

Acknowledgements This article has been produced with the financial support of the European Union under the REFRESH - Research Excellence For Region Sustainability and High-tech Industries project number CZ.10.03.01/00/22_003/0000048 via the Operational Programmed Just Transition.

Data Availability Statement This manuscript has no associated data. [Authors' comment: This is theoretical study so, no data will be deposited.]

Code Availability Statement This manuscript has no associated code/software. [Authors' comment: This is theoretical study so, no code will be provided.]

Funded by SCOAP[3].

References

1. S. Chandrasekhar, *An Introduction to the Study of Stellar Structure* (University of Chicago, Chicago, 1939)
2. R.F. Tooper, Adiabatic fluid spheres in general relativity. Astrophys. J. **142**, 1541 (1965)
3. H. Komatsu, Y. Eriguchi, I. Hachisu, Rapidly rotating general relativistic stars-I. Numerical method and its application to uniformly rotating polytropes. Mon. Not. R. Astron. Soc. **237**(2), 355–379 (1989)
4. H.J. Lane, On the theoretical temperature of the sun, under the hypothesis of a gaseous mass maintaining its volume by its internal heat, and depending on the laws of gases as known to terrestrial experiment. Am. J. Sci. **2**(148), 57–74 (1870)
5. L. Herrera, A. Di Prisco, W. Barreto, J. Ospino, Conformally flat polytropes for anisotropic matter. Gen. Relativ. Gravit. **46**, 1–16 (2014)
6. A. Kovetz, Slowly rotating polytropes. Astrophys. J. **154**, 999 (1968)
7. M.A. Abramowicz, Polytropes in N-dimensional spaces. Acta Astron. **33**(2), 313–318 (1983)
8. L. Herrera, W. Barreto, Newtonian polytropes for anisotropic matter: general framework and applications. Phys. Rev. D **87**(8), 087303 (2013)
9. L. Herrera, W. Barreto, General relativistic polytropes for anisotropic matter: the general formalism and applications. Phys. Rev. D **88**(8), 084022 (2013)
10. P.H. Chavanis, Models of universe with a polytropic equation of state: II. The late universe. Eur. Phys. J. Plus **129**(10), 222 (2014)
11. R.C. Freitas, S.V.B. Goncalves, Polytropic equation of state and primordial quantum fluctuations. Eur. Phys. J. C **74**, 1–11 (2014)
12. M. Azam, S.A. Mardan, I. Noureen, M.A. Rehman, Study of polytropes with generalized polytropic equation of state. Eur. Phys. J. C **76**, 1–9 (2016)
13. D. Santana, E. Fuenmayor, E. Contreras, Integration of the Lane-Emden equation for relativistic anisotropic polytropes through gravitational decoupling: a novel approach. Eur. Phys. J. C **82**(8), 703 (2022)
14. D. Suárez-Urango, J. Ospino, H. Hernández, L.A. Núñez, Acceptability conditions and relativistic anisotropic generalized polytropes. Eur. Phys. J. C **82**(2), 1–22 (2022)
15. N. Godani, G.C. Samanta, Neutron stars with polytropic equation of state. New Astron. **107**, 102148 (2024)
16. S.A. Mardan, A. Asif, I. Noureen, New classes of generalized anisotropic polytropes pertaining radiation density. Eur. Phys. J. Plus **134**(5), 242 (2019)
17. R.L. Bowers, E.P.T. Liang, Anisotropic spheres in general relativity. Astrophys. J. **188**, 657 (1974)
18. M. Cosenza, L. Herrera, M. Esculpi, L. Witten, Some models of anisotropic spheres in general relativity. J. Math. Phys. **22**(1), 118–125 (1981)
19. L. Herrera, N.O. Santos, Local anisotropy in self-gravitating systems. Phys. Rep. **286**(2), 53–130 (1997)
20. L. Herrera, A. Di Prisco, J. Martin, J. Ospino, N.O. Santos, O. Troconis, Spherically symmetric dissipative anisotropic fluids: a general study. Phys. Rev. D **69**(8), 084026 (2004)
21. L. Herrera, W. Barreto, Newtonian polytropes for anisotropic matter: general framework and applications. Phys. Rev. D **87**(8), 087303 (2013)
22. K.P. Reddy, M. Govender, S.D. Maharaj, Impact of anisotropic stresses during dissipative gravitational collapse. Gen. Relativ. Gravit. **47**, 1–25 (2015)
23. O.F. Bustos, Lane-Emden equations for Relativistic Anisotropic Polytropes. J. Phys. Conf. Ser. **2796**(1), 012006 (2024)
24. L. Baskey, S. Ray, S. Das, S. Majumder, A. Das, Anisotropic compact stellar solution in general relativity. Eur. Phys. J. C **83**(4), 1–13 (2023)
25. T. Cadogan, E. Poisson, Self-gravitating anisotropic fluids. I: context and overview. arXiv preprint arXiv:2406.03185 (2024)
26. S.N. Sajadi, M. Khodadi, O. Luongo, H. Quevedo, Anisotropic generalized polytropic spheres: regular 3D black holes. Phys. Dark Universe **45**, 101525 (2024)
27. Z. Stuchlík, S. Hledik, J. Novotný, General relativistic polytropes with a repulsive cosmological constant. Phys. Rev. D **94**(10), 103513 (2016)

28. H. Bondi, The contraction of gravitating spheres. Proc. R. Soc. Lond. Ser. A Math. Phys. Sci. **281**(1384), 39–48 (1964)
29. S.C. Pandey, M.C. Durgapal, A.K. Pande, Relativistic polytropic spheres in general relativity. Astrophys. Space Sci. **180**, 75–92 (1991)
30. S.A. Mardan, I. Noureen, A. Khalid, Charged anisotropic compact star core-envelope model with polytropic core and linear envelope. Eur. Phys. J. C **81**(10), 1–14 (2021)
31. M.S.R. Delgaty, K. Lake, Physical acceptability of isolated, static, spherically symmetric, perfect fluid solutions of Einstein's equations. Comput. Phys. Commun. **115**(2–3), 395–415 (1998)
32. H.A. Buchdahl, General relativistic fluid spheres. Phys. Rev. **116**(4), 1027 (1959)
33. P. Tamta, P. Fuloria, Study of anisotropic stellar objects, a revisit to Buchdahl metric potential. Int. J. Mod. Phys. D **31**(08), 2250057 (2022)
34. S.K. Maurya, A. Banerjee, M.K. Jasim, J. Kumar, A.K. Prasad, A. Pradhan, Anisotropic compact stars in the Buchdahl model: a comprehensive study. Phys. Rev. D **99**(4), 044029 (2019)
35. R.W. Romani, D. Kandel, A.V. Filippenko, T.G. Brink, W. Zheng, PSR J0952-0607: the fastest and heaviest known galactic neutron star. Astrophys. J. Lett. **934**(2), L17 (2022)
36. D.N. Spergel, L. Verde, H.V. Peiris, E. Komatsu, M.R. Nolta, C.L. Bennett, E.L. Wright, First-year Wilkinson Microwave Anisotropy Probe (WMAP)* observations: determination of cosmological parameters. Astrophys. J. Suppl. Ser. **148**(1), 175 (2003)
37. M.C. Miller, F.K. Lamb, A.J. Dittmann, S. Bogdanov, Z. Arzoumanian, K.C. Gendreau, Y. Soong, PSR J0030+ 0451 mass and radius from NICER data and implications for the properties of neutron star matter. Astrophys. J. Lett. **887**(1), L24 (2019)
38. H.T. Cromartie, E. Fonseca, S.M. Ransom, P.B. Demorest, Z. Arzoumanian, H. Blumer, W.W. Zhu, Relativistic Shapiro delay measurements of an extremely massive millisecond pulsar. Nat. Astron. **4**(1), 72–76 (2020)
39. B. Das, K.B. Goswami, P.K. Chattopadhyay, A comparative study on maximum mass and radius of compact star from Heintzmann geometry and TOV approach. arXiv preprint arXiv:2309.11468 (2023)
40. D. Bhattacharjee, P.K. Chattopadhyay, Maximum mass of an anisotropic compact object admitting the modified Chaplygin equation of state in Buchdahl-I metric. Eur. Phys. J. C **84**(1), 1–11 (2024)
41. G. Mustafa, A. Ditta, S. Mumtaz, S.K. Maurya, D. Sofuoğlu, Study on physical properties and maximum mass limit of Finch-Skea anisotropic model under Karmarkar condition in $f(Q)$-gravity. Chin. J. Phys. **88**, 938–954 (2024)
42. G. Mustafa, M.F. Shamir, X. Tie-Cheng, Physically viable solutions of anisotropic spheres in $f(R, G)$ gravity satisfying the Karmarkar condition. Phys. Rev. D **101**(10), 104013 (2020)
43. A. Malik, A. Almas, T. Naz, R. Manzoor, Physically viable solutions of anisotropic hybrid stars in $f(T)$ gravity: an embedding approach. Eur. Phys. J. Plus **139**(7), 587 (2024)
44. H. Nazar, G. Abbas, A. Abbas, S. Qaisar, Collapsing shear-free anisotropic embedding star model in $f(R)$ gravity. Fortschr. Phys. **72**(4), 2300250 (2024)
45. T. Naz, A. Malik, Z. Ramay, Physical behavior of anisotropic quark stars in modified $f(R, T)$ gravity. Int. J. Theor. Phys. **63**(3), 78 (2024)
46. T. Tangphati, I. Karar, A. Pradhan, A. Banerjee, Constraints on the maximum mass of quark star and the GW 190814 event. Eur. Phys. J. C **82**(1), 57 (2022)
47. M.C. Miller, F.K. Lamb, A.J. Dittmann, S. Bogdanov, Z. Arzoumanian, K.C. Gendreau, I. Stairs, The radius of PSR J0740+ 6620 from NICER and XMM-Newton data. Astrophys. J. Lett. **918**(2), L28 (2021)
48. W. El Hanafy, A. Awad, Implications of the conformal constraint on sound speed on the radius of PSR J0952-0607 within Rastall gravity. Astrophys. J. **951**(2), 144 (2023)
49. A. Bauswein, N. U. F. Bastian, D. Blaschke, K. Chatziioannou, J. A. Clark, T. Fischer, N. Stergioulas, Equation-of-state constraints and the QCD phase transition in the era of gravitational-wave astronomy. In *AIP Conference Proceedings* (Vol. 2127, No. 1) (AIP Publishing, 2019)
50. P.B. Demorest, T. Pennucci, S.M. Ransom, M.S.E. Roberts, J.W.T. Hessels, A two-solar-mass neutron star measured using Shapiro delay. Nature **467**(7319), 1081–1083 (2010)
51. M. Linares, T. Shahbaz, J. Casares, Peering into the dark side: Magnesium lines establish a massive neutron star in PSR J2215+ 5135. Astrophys. J. **859**(1), 54 (2018)
52. T. Güver, F. Özel, A. Cabrera-Lavers, P. Wroblewski, The distance, mass, and radius of the neutron star in $4U\,1608-52$. Astrophys. J. **712**(2), 964 (2010)
53. C.A. Kolassis, N.O. Santos, D. Tsoubelis, Energy conditions for an imperfect fluid. Class. Quantum Gravity **5**(10), 1329 (1988)
54. S.W. Hawking, G.F. Ellis, *The Large Scale Structure of Space-Time* (Cambridge University Press, Cambridge, 2023)
55. R. Wald, *General Relativity* (University of Chicago Press, Chicago, 1984)
56. B.P. Brassel, S.D. Maharaj, R. Goswami, Inhomogeneous and radiating composite fluids. Entropy **23**(11), 1400 (2021)
57. B..P. Brassel, S..D. Maharaj, R. Goswami, Higher-dimensional inhomogeneous composite fluids: energy conditions. Prog. Theor. Exp. Phys. **2021**(10), 103E01 (2021)
58. R.C. Tolman, Static solutions of Einstein's field equations for spheres of fluid. Phys. Rev. **55**(4), 364 (1939)
59. J.R. Oppenheimer, G.M. Volkoff, On massive neutron cores. Phys. Rev. **55**(4), 374 (1939)
60. Ø. Grøn, Repulsive gravitation and electron models. Phys. Rev. D **31**(8), 2129 (1985)
61. L. Herrera, Cracking of self-gravitating compact objects. Phys. Lett. A **165**(3), 206–210 (1992)
62. H. Abreu, H. Hernández, L.A. Núnez, Sound speeds, cracking and the stability of self-gravitating anisotropic compact objects. Class. Quantum Gravity **24**(18), 4631 (2007)
63. J. Rafelski, C. Dietl, L. Labun, Compact ultradense objects in the solar system. arXiv preprint arXiv:1303.4506 (2013)
64. C. Dietl, L. Labun, J. Rafelski, Properties of gravitationally bound dark compact ultra dense objects. Phys. Lett. B **709**(3), 123–127 (2012)
65. R. Tamta, P. Fuloria, P. Tamta, Models of super dense structures using a new form of the mass function. J. Phys. Sci. Eng. Technol. **14**(02), 187–194 (2022)
66. R. Carballo-Rubio, Stellar equilibrium in semiclassical gravity. Phys. Rev. Lett. **120**(6), 061102 (2018)
67. P.V. Cunha, C. Herdeiro, E. Radu, N. Sanchis-Gual, Exotic compact objects and the fate of the light-ring instability. Phys. Rev. Lett. **130**(6), 061401 (2023)